Wavelet Transform Based Relay Algorithm for the Detection of Stochastic High Impedance Faults

T. M. Lai[1], L.A. Snider[1] and E. Lo[1]

(1) Dept. of Electrical Engineering, The Hong Kong Polytechnic University, Hung Hom, Kowloon, Hong Kong, (e-mail: tmlai.ee@polyu.edu.hk, eesnider@polyu.edu.hk, eewclo@polyu.edu.hk)

Abstract – **High impedance faults (HIF) are faults which are difficult to detect by overcurrent protection relays. This paper presents a practical pattern recognition based algorithm for electric distribution high impedance fault detection. The scheme recognizes the distortion of the voltage and current waveforms caused by the arcs usually associated with HIF. The analysis using Discrete Wavelet Transform (DWT) yields three phase voltage and current in the low frequency range which fed to a classifier for pattern recognition. The classifier is based on the algorithm using nearest neighbour rule approach. A HIF model was also developed, where the random nature of the arc was simulated using MATLAB.**

Keywords – High Impedance Faults, Wavelet Transform, Pattern Recognition

I. INTRODUCTION

High impedance faults (HIF) are difficult to detect. When a conductor such as a distribution line makes contact with a poor conductive surface or substance the resulting level of fault current is usually lower than the nominal current of the system at the fault location. Therefore, conventional protection relay system will not be able to detect the HIFs and trip the protection relay. The failure of HIF detection may lead to potential hazards to human beings and potential fire [1].

HIFs on electrical transmission and distribution networks involve arcing and/or nonlinear characteristics of fault impedance which cause cyclical pattern and distortion. Therefore, the objective of most detection schemes is to evaluate the special features in patterns of the voltages and currents in HIFs.

Some researchers proposed various detection schemes based on fractal techniques [2], digital signal processing [3], expect systems [4]-[5], neural networks [6]-[8], crest factor [9], wavelet transform in high frequency noise patterns [10] and dominant harmonic vectors [11] [12]. They offer potential solutions to these problems currently associated with conventional schemes. While direct calculation of fractal dimensions is not effective due to relatively short data sets available for estimation, the use of high frequency harmonics is not feasible in practical relay because of the filtering by substation current transformers. The scheme proposed in this paper, which uses the nearest neighbour rule approach, offers a simpler pattern recognition alternative to recognise the distortion due to HIFs. Moreover, these schemes can also potentially be applied on on-line training and customization using actual field HIF data. This proposed detection scheme needs evaluation on merely low order harmonics of voltage and current.

In this paper a stochastic method applied towards the detection of HIFs is presented. The method incorporates the statistical nature of the high impedance faults and fault locations in order to predict the distortions on voltage and current waveform in the electrical supply network. The immunity of the proposed relay to confounding from contingencies such as load and capacitor switching in electrical networks is evaluated through simulation. After capturing the voltage and current waveforms from the power system simulations, they are analysed by discrete wavelet transform (DWT) to produce various waveforms under different frequency ranges. The rms values of these voltage and current waveforms in their various frequency ranges are fed into the pattern classifier to determine the fault or non-fault situations.

II. DISCRETE WAVELET TRANSFORM (DWT) MODEL AND MULTI-RESOLUTION ANALYSIS (MRA)

The wavelet transform is a tool that divides up data, functions or operators into different frequency components, and then studies each component with a resolution matched to its scale [13]. The multi-resolution analysis (MRA) using discrete wavelet transform (DWT) in wavelet is used in this proposed method. The objective of multi-resolution analysis is to develop representations of a sophisticated signal *f(t)* in terms of wavelet and scaling function. Multi-resolution analysis was formulated based on the study of orthonormal, compactly supported wavelet bases. Wavelets theory and its applications are rapidly developing fields in applied mathematics and signal analysis.

The scaling coefficients (approximation) can be computed by taking the inner products of the function *f(t)* with the scaling basis:

$$c_{j,k} = \langle f(t), \phi_{j,k}(t) \rangle = \int_{-\infty}^{\infty} f(t)\phi_{j,k}(t)dt \qquad (1)$$

The wavelet coefficients (details) can be computed by taking the inner products of the function *f(t)* with the wavelet basis:

$$d_{j,k} = \langle f(t), \psi_{j,k}(t) \rangle = \int_{-\infty}^{\infty} f(t)\psi_{j,k}(t)dt \qquad (2)$$

where scale function $\phi_{j,k}(t)$ and wavelet function $\psi_{j,k}(t)$ is determined by the selection of a particular mother wavelet $\psi(t)$ and the following equations.

$$\phi_{j,k}(t) = 2^{j/2}\phi(2^j t - k)$$
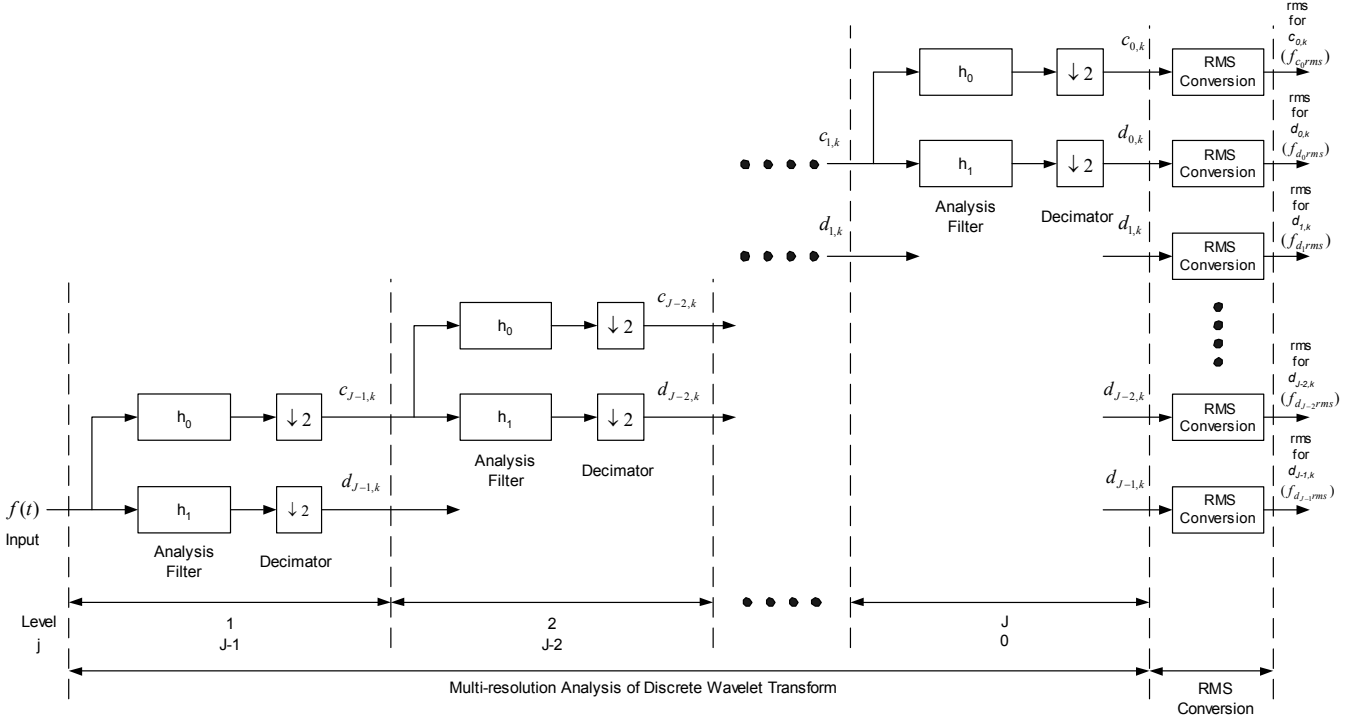$$\psi_{j,k}(t) = 2^{j/2}\psi(2^j t - k) \qquad (3)$$

Fig 1. Schematic Diagram of Discrete Wavelet Transform (DWT)

The schematic diagram of DWT is shown in Fig 1. Discrete Wavelet Transform (DWT) resolves the input signal to time, scales and scale coefficients and wavelet coefficients. The scales, scale coefficients and wavelet coefficients are not commonly used because they cannot reflect the physical properties in the frequency analysis. Therefore, these following sections would introduce some mappings from scale and scale coefficients and wavelet coefficients to frequency ranges and rms values of scale coefficients and wavelet coefficients in each DWT resolution levels, respectively.

A. Mapping from Scales to Frequency Ranges

In discrete wavelet transform, resolution scale is commonly used to represent the degree of resolution. The structure of DWT is shown in Fig 1. Two definitions of resolution level are commonly used: ascending order *Level* from the finest resolution level (1) to the coarsest resolution level (*J*) and descending order *j* from the finest resolution level (*J*-1) to the coarsest resolution level (0) where *J* is total resolution level. The relationship between *Level* and *j* is defined as follows:

$$Level = J - j \tag{4}$$

and the resolution levels in terms of *Level* and *j* are listed at the bottom of Fig 1. The resolution scale $scale_{Level}$ in each resolution level is defined as:

$$scale_{Level} = 2^{Level} \tag{5}$$

In each resolution level, the input signal d_{j+1} in the upper resolution level is split into the approximation c_j by a lowpass filter h_0 and the detail d_j by the highpass filter h_1 in the lower resolution level. Both of output approximation and detail signal are then decimated by 2. Based on the Nyquist theorem (which states that the highest frequency which can be accurately represented is less than one-half of the sampling rate), the maximum frequency of original

signal *f(t)* sampled at $freq_{f(t)}$ Hz is $freq_{f(t)}/2$ Hz. The first approximation c_{J-1} and first detail d_{J-1} in resolution level 1 are sampled at half of $freq_{f(t)}$. Therefore, the maximum frequencies $freq_{Level}$ of signals c_j and d_j in each resolution level *Level* are given in Equation 6:

$$freq_{Level} = \frac{freq_s}{2^{Level}} \tag{6}$$

Since the boundary of lowpass and highpass filter is half of nyquist frequency, the upper boundary frequency of lowpass filter h_0 and the lower boundary frequency of highpass filter h_1 is the same as half of $freq_{Level}$. Therefore, the lower boundary frequency $freq_{Lower}$ and upper boundary frequency $freq_{Upper}$ of both lowpass filter h_0 and highpass filter h_1 in each resolution level *Level* are defined as:

$$\begin{aligned} freq_{Lower} &= 0 \\ freq_{Upper} &= \frac{freq_{f(t)}}{2^{Level+1}} \end{aligned} \quad \text{for lowpass filter} \tag{7}$$

$$\begin{aligned} freq_{Lower} &= \frac{freq_{f(t)}}{2^{Level+1}} \\ freq_{Upper} &= \frac{freq_{f(t)}}{2^{Level}} \end{aligned} \quad \text{for highpass filter.} \tag{8}$$

B. Calculation of RMS values from Scale/Wavelet Coefficients

Scale coefficients and wavelet coefficients $coeff_{signal}$ representing the distorted signal *f(t)* at different resolution levels in multi-resolution analysis (MRA) are defined as:

Low Frequency Range $\Rightarrow$ High Frequency Range

$$coeff_{signal} = \left[c_0 \,|\, d_0 \,|\, d_1 \,|\, ... \,|\, d_{J-2} \,|\, d_{J-1} \right] \tag{9}$$

where *J* is maximum level in this multi-resolution analysis and c_0 and d_j are the approximation in level 0 and the detail in level *j* respectively.

For the periodic mode of discrete wavelet transform, the

rms values of their scale coefficients and wavelet coefficients can be calculated directly from their scale coefficients and wavelet coefficients in their own resolution levels.

The rms values for the details or approximation in each wavelet level can be represented in the periodic-padding (periodic extension at the edges) mode of discrete wavelet transform. For the scale coefficient in level J ($j = 0$), the rms value f_{c0rms} in level J ($j = 0$) is:

$$f_{c_0 rms} = \sqrt{\frac{\|f_{c0}(t)\|_2^2}{L_{f(t)}}} = \sqrt{\frac{\sum_k c_0(k)^2}{2^J L_{c_o}}} \qquad (10)$$

$$L_{f(t)} = 2^J L_{c_o}$$

where $L_{f(t)}$ is no. of points in $f(t)$ and

L_{c_o} is no. of points in scale coefficient c_0.

For the wavelet coefficients in each level, the rms values f_{djrms} in level j are:

$$f_{d_j rms} = \sqrt{\frac{\|f_{dj}(t)\|_2^2}{L_{f(t)}}} = \sqrt{\frac{\sum_k d_j(k)^2}{2^{Level} L_{d_j}}} = \sqrt{\frac{\sum_k d_j(k)^2}{2^{J-j} L_{d_j}}}$$

$$L_{f(t)} = 2^{Level} L_{d_j} = 2^{J-j} L_{d_j} \qquad (11)$$

where L_{d_j} is no. of points in wavelet coefficients d_j

Therefore, the rms vector rms_{signal} representing to scale coefficients and wavelet coefficients of the distorted signal $f(t)$ at different resolution levels is as follows:

$$rms_{signal} = \left[f_{c_0 rms} \mid f_{d_0 rms} \mid f_{d_1 rms} \mid \ldots \ldots \mid f_{d_{J-2} rms} \mid f_{d_{J-1} rms} \right]$$

$$rms_{signal} = \left[\sqrt{\frac{\sum_k c_0(k)^2}{2^J L_{c_o}}} \middle| \sqrt{\frac{\sum_k d_0(k)^2}{2^J L_{d_0}}} \right.$$

$$\left. \sqrt{\frac{\sum_k d_1(k)^2}{2^{J-1} L_{d_1}}} \middle| \ldots \ldots \middle| \sqrt{\frac{\sum_k d_{J-2}(k)^2}{2^2 L_{d_{J-2}}}} \middle| \sqrt{\frac{\sum_k d_{J-1}(k)^2}{2 L_{d_{J-1}}}} \right] \qquad (12)$$

In accordance with the above equations, the rms values calculated from scale coefficients and wavelet coefficients in multi-resolution levels can convert directly from their scale coefficients and wavelet coefficients $coeff_{signal}$.

III. MODELLING AND THEIR THEORIES

A. Simulation Model Procedures

The system model of this simulation was divided into three parts: power system model, filter model and pattern recognition model. Fig 2 shows the flowchart of the simulation. Matlab was used to generate all the system parameters in the fault cases and non-fault cases for the power system simulation according to random fault location and fault situations. The system parameters in fault and non-fault cases were then imported into the power system simulation and the power system toolbox determined the targeted voltage and current waveforms of the circuit breaker in the faulted distribution line. These waveforms of voltages and currents in the relay on the distribution side of the transformer in the power system studied were then transferred to discrete wavelet transform progress to analyse the frequency characteristics in various frequency ranges. The rms values of that voltages and currents were calculated using the voltage and current waveforms from the discrete wavelet transform. A classifier was used to recognize the fault cases and non-fault cases using rms values of voltage and current in various frequency bands.
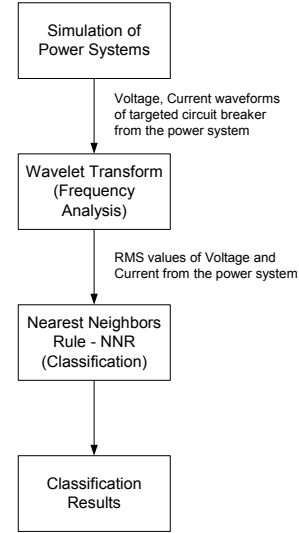

Fig 2. Simulation Model Procedures – Matlab Application

B. Power System Model - High Impedance Faults (HIFs) and Low Impedance Faults (LIFs) Model

A simplified 2-diode model [14] of HIF is used in the simulation. The circuit of the HIFs model is shown in Fig 3. This HIF model is based on arcing in sandy soil. The model includes two DC sources, Vp and Vn, which represent the inception voltage of air in soil and/or between trees and the distribution line. The two resistances, Rp and Rn, represent the fault resistance: unequal values allow for asymmetric fault currents to be simulated. When the phase voltage is greater than the positive DC voltage Vp, the fault current flows towards the ground. The fault current reverses when the line voltage is less than the negative DC voltage Vn. For values of the phase voltage between Vn and Vp no fault current flows. The typical fault current and voltage are shown in Fig 4.

The low impedance fault (LIF) model comprises the appropriate fault resistance switched at the fault location in the distribution line.
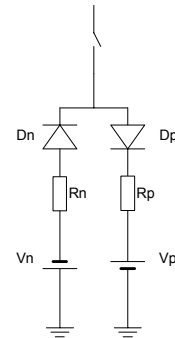

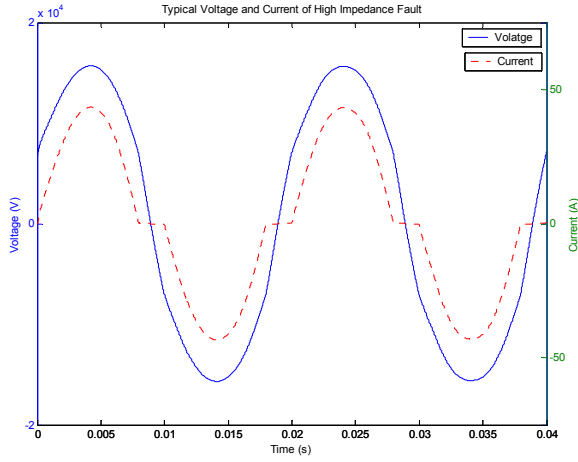Fig 3. Simplified 2-diode Fault Model of HIF

Fig 4. Typical Voltage and Current of HIF

C. Implementation of Discrete Wavelet Transform (DWT) Model and Multi-resolution Analysis (MRA)

In this application, db4 in Daubechies family wavelets is selected for the mother wavelet and the frequency bandwidths were determined in Table 1 after downsampling the input signal $f(t)$ to the sampling frequency of 9600Hz in order to reduce the computational time.

Table 1 : Scale to Frequency Range Conversion based on 50Hz Power Frequency

Level	Parameter	Frequency Band (Hz)	Harmonics Included
6	$c_{0,k}$	0 – 75	1st
6	$d_{0,k}$	75 – 150	$2^{nd} – 3^{rd}$
5	$d_{1,k}$	150 – 300	$3^{rd} – 6^{th}$
4	$d_{2,k}$	300 - 600	$6^{th} – 12^{th}$
3	$d_{3,k}$	600 - 1200	$12^{th} - 24^{th}$
2	$d_{4,k}$	1200 - 2400	$24^{th} – 48^{th}$
1	$d_{5,k}$	2400 - 4800	$48^{th} – 96^{th}$

D. Pattern Recognition

Since the normal operation and fault situations do not have a specific pattern for the distributions, a nonparametric approach in supervised learning is used in this fault classification problem. The nearest neighbour rule (NNR) method [15] [16] is a typical recognition method in the nonparametric approach. The NNR method is initially used to select some samples randomly from the data to be classified as a training set of labelled samples $\vec{x}_{train}$. Since samples which are close in feature space likely belong to the same class, a new sample $\vec{x}_0$ in the training grid is selected and labelled to be the same class as the nearest labelled samples $\vec{x}_i$ in the training set of $\vec{x}_{train}$. NNR can demonstrate the classification results and their decision boundaries between two sorts of data by plotting two-dimensional contour graphs.

The root-mean-square values of voltages and currents in various frequency ranges from the DWT are classified into a training set and a test set respectively. 95% of the rms values are used as a training set to train the decision boundaries using NNR and the rest of the data acts as a test set to validate their decision boundaries.

IV. SYSTEM DESCRIPTION

Three systems studied in this paper are parts of 25kV power distribution networks. A distribution network with a single branch of a nonlinear load, a radial distribution network with three branches of nonlinear loads and one meshed network with two sources and various nonlinear loads are described and their schematic diagrams are shown in Fig 5, 6 and 7, respectively.
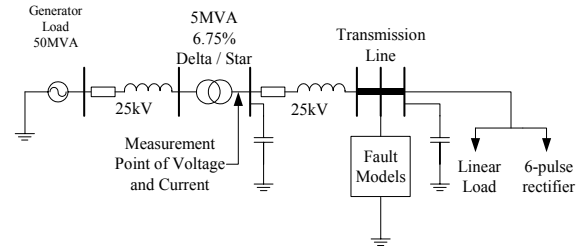

Fig 5. Schematic Diagram of the Simulated 25kV Single Branch Power System Network
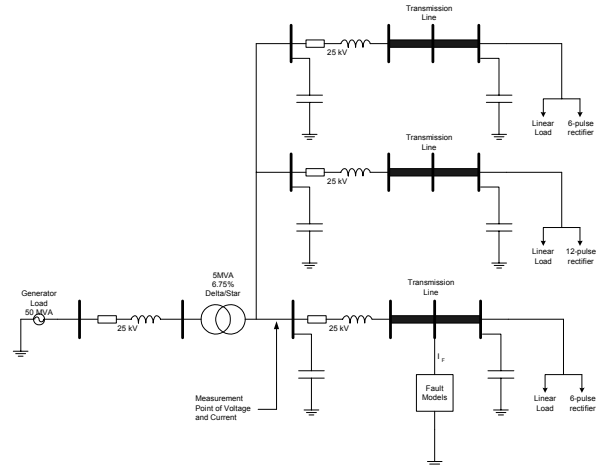

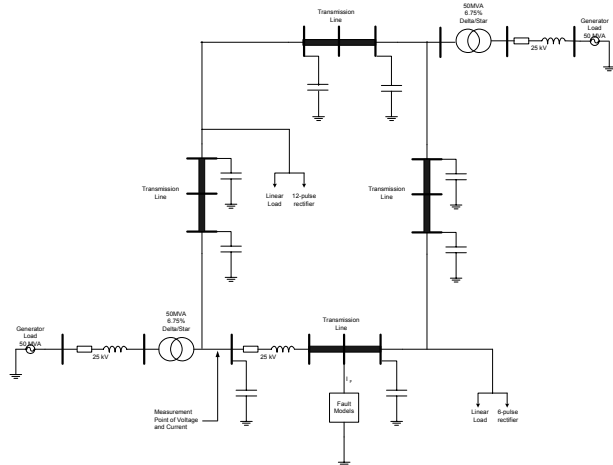Fig 6. Schematic Diagram of the Simulated 25kV Radial Power System Network

Fig 7. Schematic Diagram of the Simulated 25kV Meshed Power System Network

In the single branch distribution network, power is supplied at 25 kV through a 20km distribution line from a 5 MVA transformer. The network then distributes power to a 4 MVA linear load with power factor 0.8 and a 1 MVA nonlinear load, where a 6 pulse converter is used to represent the nonlinear load. In the radial distribution network with three branches of nonlinear loads, two additional branches of one 2 MVA 6 pulse converter load and one 4.262 MVA 12 pulse converter load are parallel to the distribution branch in the single branch distribution network. In the meshed network, a ring connection is constructed by two separate 3 phase voltage sources feeding two individual nonlinear loads with one 1 MVA 6 pulse converter load and one 4.262 MVA 12 pulse converter load. The resistance, inductance and capacitance of positive and zero sequence of transmission lines are R_1 = 0.01273 ohm/km; X_1 = 1.334 mH/km; C_1 = 0.00833 µF/km and R_0 = 0.3864 ohm/km; X_0 = 2.496 mH/km; C_0 = 0.00641 µF/km, respectively. The total impedance percentage of the transformers is 6.75% and the frequency of the system is 50Hz.

In this paper, two sorts of cases are considered in the simulation: 1000 non-fault cases and 1000 fault cases in each system. In fault cases, both high impedance fault model and low impedance fault model are applied separately to the distribution line for different fault cases. The arcing and nonlinear characteristics of HIFs may be similar to those of nonlinear loads and switching operations, especially capacitor switching. It must be ensured that these normal events do not confound the HIF relay. In the simulations, the significant parameters are stochastically selected based on those in real operations. The fault currents are assumed to range from 0.25 to 2 p.u. of overcurrent device settings in full load situation.

A. Case I – Non-fault Cases (Normal Operation)

In all distribution networks, shunt capacitors banks ranging up to 1 MVAr, linear loads up to their own maximum powers and nonlinear loads up to their own maximum ratings are switched at the sending end and receiving end of the distribution lines. The nonlinear loads comprise three phase 6 pulse converters and 12 pulse converters and the three phase linear loads have their own power factor in accordance with their system configurations. The closing times of the breakers are stochastically selected.

B. Case II – Fault Cases

The modelled phase-to-ground HIFs and LIFs with various fault inception angles are simulated at the different positions along the faulted distribution lines from the circuit breaker at the source side to distribution loads. Fault location, fault impedance and fault inception angles of both HIFs and LIFs are stochastically selected in the simulation which represents the variation of soil properties and other stochastic characteristics of the HIFs. The capacities of the linear loads and the nonlinear loads, operation schedule in the capacitors at the sending end and receiving end in the distribution lines of the simulated distribution networks are chosen randomly.

V. SIMULATION

Table 2 are total errors $error_{total}$ in the NNR method. In the pattern recognition, the fault cases and non-fault cases are classified into the training set, test set in the simulation. The probability errors in pattern recognitions were found that lower probability errors mean higher successful rates to classify the two above cases.

The total errors show average errors on each combination of wavelet coefficients. The errors of corresponding to rms values of voltage wavelet coefficients ($d_{0,k}$) in level 6 are still approximately between 2.52% and 16.80% which is the lowest value in all combinations of various frequency ranges in voltage and current. Moreover, the range of total errors is from 2.52% and 45.4%.

It noted that the major characteristic in recognizing of normal operation and fault cases is the combinations on voltages ranged from 0 to 300 Hz and currents ranged from 0 to 600 Hz. Therefore, voltages and currents with low frequency ranges are major factors to classify the high impedance faults and the common faults.

Although the decision boundaries could verify all cases of the simulated systems, some occurrences of these high impedance faults beyond the simulated cases may still occur. Since high impedance faults constitute a fault period in terms of seconds, tripping criteria are required. Positive identifications in ten consecutive cycles of HIFs triggered by the trained pattern classifier could classify an event as a high impedance fault.

VI. CONCLUSIONS

This paper presented a study of the fault classification in 25kV electrical distribution systems based on discrete wavelet transform. The study involved computer simulation of power systems, discrete wavelet transform and classification. The electrical faults including HIFs and common faults are stochastic in nature, and depend on factors such as fault location, fault impedance, fault inception angle, other electrical loads, etc. A statistical analysis was performed, and this determined the error probability of classification between the fault cases and normal operation. The statistical data was incorporated into the computer simulation, and the classification results identified both the fault cases and normal operation. The difference of frequency characteristics between high impedance faults and normal capacitor bank switching operation simulated by MATLAB can be recognized by the classifier using nearest neighbor rule method. Computer simulations for the proposed method in three example power systems indicated that the method provided a satisfactory results in the detection of HIF.

The method presented in this paper overcomes the difficulty of using discrete wavelet transform that the output scale coefficients and wavelet coefficients do not represent any physical properties. Using the relationship among scale coefficients and wavelet coefficients, signal energies and rms values, scale coefficients and wavelet coefficients can be converted to rms values directly or through the calculation of signal energies. Therefore, the clear distribu-

tion patterns among various characteristic voltage and current rms values calculated from scale coefficients and wavelet coefficients are demonstrated.

VII ACKNOWLEDGEMENT

VIII. REFERENCES

[1] IEEE Tutorial Course Text, Detection of Downed Conductors on Utility Distribution Systems, No. 90EH0310-3-PWR, 1989

[2] A.V. Mamishev, B.D. Russell, C.L. Benner, "Analysis of High Impedance Faults using Fractal Techniques," IEEE Power Industry Computer Application Conference, 1995, pp 401 - 406

[3] A.A. Girgas, W.Chang, E.B. Makram, "Analysis of High-Impedance Fault Generated Signals using a Kalman Filtering Approach," IEEE Transactions on Power Delivery, Volume 5 Issue: 4 , Oct. 1990, pp 1714 -1724

[4] C.J. Kim, B.D. Russell, "Classification of Faults and Switching Events by Inductive Reasoning and Expert System Methodology," IEEE Transactions on Power Delivery, Volume 4, Issue 3, July 1989, pp 1631 -1637

[5] B.D. Russell, C.L. Benner, "Arcing Fault Detection for Distribution Feeders: Security Assessment in Long Term Field Trials," IEEE Transactions on Power Delivery, Volume 10, Issue 2, April 1995, pp 676 – 683

[6] S. Ebron, D.L. Lubkeman, M. White, "A Neural Network Approach to the Detection of Incipient Faults on Power Distribution Feeders" IEEE Transactions on Power Delivery, Volume 5, Issue 2, April 1990, pp 905 -914

[7] L.A. Snider, Y.S. Yuen, "The Artificial Neural Networks Based Relay for the Detection of Stochastic High Impedance Faults", Neurocomputing, Volume 23, 1998, pp 243-254

[8] A.M. Sharaf, L.A. Snider, K. Debnath, "A Neural Network Based Relaying Scheme for Distribution System High Impedance Fault Detection," Proceedings of First New Zealand International Two-Stream Conference on Artificial Neural Networks and Expert Systems, 1993, pp 321 -324

[9] C.J. Kim, B.D. Russell, "Analysis of Distribution Disturbances and Arcing Faults Using the Crest Factor," Electric Power Systems Research, Volume 35, 1995, pp141-148

[10] David T.W. Chan, Xia Yibin, "A Novel Technique For High Impedance Fault Identification," IEEE Transactions on Power Delivery, Volume 13, Issue 3, July 1998 pp 738 - 744

[11] B.M. Aucoin, B. D. Russell, "Detection of Distribution High Impedance Faults Using Burst Noise Signals Near 60 Hz," IEEE Transactions on Power Delivery, Volume 2, Issue 2, April 1987, pp 342 - 348

[12] D.I. Jeerings, J.R. Linders, "A Practical Protective Relay for Down-conductor Faults," IEEE Transactions on Power Delivery, Volume 6, Issue 2, April 1991, pp 565 -574

[13] I. Daubechies, *Ten lectures on wavelets*, Philadelphia, Pa. : Society for Industrial and Applied Mathematics, 1992

[14] A.E. Emanuel, D. Cyganski, J.A. Orr, S. Shiller, E.M. Gulachenski, "High Impedance Fault Arcing on Sandy Soil in 15 kV Distribution Feeders: Contributions to the Evaluation of the Low Frequency Spectrum," IEEE Transactions on Power Delivery, Volume 5, Issue 2, April 1990 pp 676 -686

[15] M. Nadler, E.P. Smith, *Pattern Recognition Engineering*, Wiley, 1993

[16] Duda, O. Richard, *Pattern Classification*, Wiley, 2001

Table 2. Total Error Percentages in Various Wavelet Scales

	V_{scale0} $c_{0,k}$	$V_{wavelet0}$ $d_{0,k}$	$V_{wavelet1}$ $d_{1,k}$	$V_{wavelet2}$ $d_{2,k}$	$V_{wavelet3}$ $d_{3,k}$	$V_{wavelet4}$ $d_{4,k}$	$V_{wavelet5}$ $d_{5,k}$	I_{scale0} $c_{0,k}$	$I_{wavelet0}$ $d_{0,k}$	$I_{wavelet1}$ $d_{1,k}$	$I_{wavelet2}$ $d_{2,k}$	$I_{wavelet3}$ $d_{3,k}$	$I_{wavelet4}$ $d_{4,k}$	$I_{wavelet5}$ $d_{5,k}$
V_{scale0} $c_{0,k}$	-	16.80	3.55	7.98	11.52	9.47	9.27	4.88	4.67	8.60	8.92	9.15	9.15	9.15
$V_{wavelet0}$ $d_{0,k}$	16.80	-	3.50	8.03	10.18	10.65	10.27	5.15	4.98	3.22	2.52	9.83	10.18	10.20
$V_{wavelet1}$ $d_{1,k}$	3.55	3.50	-	9.35	11.07	11.07	10.32	4.58	4.70	3.45	7.48	11.53	11.67	11.40
$V_{wavelet2}$ $d_{2,k}$	7.98	8.03	9.35	-	32.07	35.32	32.67	9.95	9.25	6.82	14.08	21.93	21.90	22.23
$V_{wavelet3}$ $d_{3,k}$	11.52	10.18	11.07	32.07	-	41.78	43.63	12.48	12.38	7.73	16.05	27.37	32.02	32.15
$V_{wavelet4}$ $d_{4,k}$	9.47	10.65	11.07	35.32	41.78	-	40.83	13.28	12.75	8.17	18.07	27.43	28.53	29.98
$V_{wavelet5}$ $d_{5,k}$	9.27	10.27	10.32	32.67	43.63	40.83	-	15.87	14.60	12.15	20.85	30.00	32.38	45.40
I_{scale0} $c_{0,k}$	4.88	5.15	4.58	9.95	12.48	13.28	15.87	-	11.42	6.85	8.93	12.68	13.67	14.43
$I_{wavelet0}$ $d_{0,k}$	4.67	4.98	4.70	9.25	12.38	12.75	14.60	11.42	-	7.15	8.35	11.70	13.15	15.68
$I_{wavelet1}$ $d_{1,k}$	8.60	3.22	3.45	6.82	7.73	8.17	12.15	6.85	7.15	-	6.38	9.85	12.42	7.75
$I_{wavelet2}$ $d_{2,k}$	8.92	2.52	7.48	14.08	16.05	18.07	20.85	8.93	8.35	6.38	-	19.48	22.78	20.93
$I_{wavelet3}$ $d_{3,k}$	9.15	9.83	11.53	21.93	27.37	27.43	30.00	12.68	11.70	9.85	19.48	-	31.08	33.93
$I_{wavelet4}$ $d_{4,k}$	9.15	10.18	11.67	21.90	32.02	28.53	32.38	13.67	13.15	12.42	22.78	31.08	-	33.87
$I_{wavelet5}$ $d_{5,k}$	9.15	10.20	11.40	22.23	32.15	29.98	45.40	14.43	15.68	7.75	20.93	33.93	33.87	-